Journal of Magnetism and Magnetic Materials 474 (2019) 522–527

Contents lists available at ScienceDirect

Journal of Magnetism and Magnetic Materials

journal homepage: www.elsevier.com/locate/jmmm

Research articles

Magnetic parameters evaluation of magnetic nanoparticles for use in biomedical applications

Ahmed L. Elrefai[a,b,*], Takashi Yoshida[b], Keiji Enpuku[b]

[a] Department of Electrical Power and Machines, Cairo University, Giza 12613, Egypt
[b] Department of Electrical and Electronic Engineering, Kyushu University, Fukuoka 819-0395, Japan

ARTICLE INFO

Keywords:
Magnetic nanoparticle
Magnetization curve
AC susceptibility
Magnetic-core size distribution
Anisotropy energy constant
Néel relaxation

ABSTRACT

We present a procedure for the comprehensive evaluation of parameters of magnetic nanoparticles (MNPs), such as saturation magnetization, core-size distribution, anisotropy energy constant, and characteristic time for Néel relaxation for use in biomedical applications and fundamental MNPs research. The static magnetization curve of suspended and immobilized MNP samples and the AC susceptibility of immobilized samples were used for the evaluation of these parameters. The magnetic properties reconstructed from the obtained parameters agreed with the experimental results, indicating the accuracy of the estimation procedure. Using the procedure, the parameters of the commercial Resovist MNP sample were evaluated. Then, the Resovist sample was magnetically fractionated into two MNP samples with large and small core sizes, and the parameters of the two fractionated samples were evaluated. It was demonstrated that the parameters of the Resovist sample are given by the volume-weighted average for those of the fractionated samples.

1. Introduction

Magnetic nanoparticles (MNP) have been widely studied for use in biomedical applications, such as hyperthermia and magnetic particle imaging (MPI) [1–4]. The key parameters that determine MNP performance in these applications are their magnetic moment m and relaxation time τ [5,6]. The value of m determines the signal strength and nonlinearity. Large m value is desired to obtain rich harmonic signals in MPI and large hysteresis loss in hyperthermia. The value of τ determines the response to high-frequency field, and appropriate τ value is required depending on the frequency of the external field used. Therefore, it is necessary to choose MNP with proper values of m and τ for specific biomedical application.

It is known that m and τ values are determined by the parameters of the MNP. The value of m is determined by the saturation magnetization M_s and magnetic core size d_c. The relaxation time τ is determined by the Brownian relaxation time τ_B or the Néel relaxtion time τ_N. The Brownian relaxation time τ_B is governed by the hydrodynamic diameter d_H of particle, viscosity η of surrounding medium, and temperature T. The τ_N value is determined by the anisotropy energy constant K, d_c, T, and the characteristic time τ_0. Therefore, it is necessary to obtain these parameters to quantitatively evaluate m and τ.

Among these parameters, η and T are usually known. The hydrodynamic diameter d_H can be obtained using an optical method, such as dynamic light scattering (DLS) method [7,8]. The remaining parameters M_s, d_c, K, and τ_0 are estimated from the magnetic properties of MNP sample. The M-H curve of suspended MNP sample can be used to evaluate the values of M_s and d_c. The distribution of d_c in MNP sample can also be evaluated by comparing the experimental M-H curve with the theoretical one based on the Langevin function [7–11]. The value of K can be evaluated from the temperature and frequency dependence of the susceptibility of immobilized MNP sample [12–14]. The M-H curve of immobilized MNP sample can also be used to evaluate K [15–17].

In this paper, we present a procedure for the comprehensive evaluation of the magnetic parameters M_s, d_c, K, and τ_0. For this purpose, we use the M-H curve of suspended and immobilized MNP samples to evaluate the values of M_s, d_c, and K. We also use the AC susceptibility (ACS) of immobilized MNP sample to evaluate the value of τ_0. First, we explain the evaluation procedure using a single-core SHP20 MNP sample (Ocean Nanotech), which has narrow size distribution. The validity of the evaluation procedure was demonstrated using this sample.

Then, we use the proposed procedure to evaluate the parameters of a multi-core Resovist MNP sample (FUJIFILM RI Pharma), which is known to have admirable performance in both hyperthermia and MPI applications [18,19]. As the Resovist MNP sample has wide size distribution, the original Resovist sample was magnetically fractionated into two MNP samples with narrow size distributions: one sample with

* Corresponding author at: Department of Electrical and Electronic Engineering, Kyushu University, Fukuoka 819-0395, Japan.
E-mail address: a.lotfyelrefai@gmail.com (A.L. Elrefai).

https://doi.org/10.1016/j.jmmm.2018.11.022
Received 9 May 2018; Received in revised form 23 September 2018; Accepted 4 November 2018
Available online 05 November 2018
0304-8853/

smaller core size and another sample with larger core size. The parameters of the two fractionated samples were evaluated using the proposed procedure. It was demonstrated that the parameters of Resovist MNP are given by volume-weighted average for those of the fractionated samples.

2. Evaluation procedure of MNP magnetic parameters

For homogeneously magnetized spherical MNP, the magnetic moment m and the Néel relaxation time τ_N are expressed as [20,21]

$$m = M_s V_c \tag{1}$$

$$\tau_N = \tau_0 \frac{\sqrt{\pi}}{2} \frac{1}{\sqrt{\sigma}} \exp(\sigma) \text{ for } \sigma > 2 \tag{2}$$

where,

$$\sigma = \frac{KV_c}{k_B T}, \quad V_c = \frac{\pi}{6} d_c^3 \tag{3}$$

We note that MNP with relatively large core size are used for MPI and hyperthermia applications, and the condition $\sigma > 2$ in Eq. (2) can be satisfied for these MNP.

We start with evaluating the parameters M_s, d_c, K, and τ_0, which determine m and τ_N as shown in Eqs. (1)–(3). In the experiment, we used the commercial SHP20 MNP sample. The nominal core size was $d_c = 20$ nm, and the iron concentration of the original sample was 5 mg (Fe)/mL. For the *M-H* curve measurement of suspended sample, 100 μL of the original SHP20 magnetic fluid were diluted in 50 μL of purified water. The immobilized MNP sample was prepared by diluting 100 μL of the original SHP20 magnetic fluid in 180 mg of liquid epoxy resin. Then, the sample was left for 12 h to immobilize via solidification.

2.1. Saturation magnetization and core size distribution

The value of M_s and d_c distribution were obtained by analyzing the static *M-H* curve of suspended MNP samples. In the experiment, *M-H* curve was measured up to $\mu_0 H = 1$ T with measurement time of 30 min. The measurement was performed using equipment constructed in the laboratory based on the conventional sample vibration scheme; the sample vibration frequency was 7 Hz.

Fig. 1(a) shows the measured *M-H* curve of the SHP20 sample at low fields. It is well known that the *M-H* curve of suspended MNP samples can be described by the Langevin function as follows [7–11]:

$$M = \int_0^\infty n_m(m) m L(\xi) dm \tag{4}$$

with

$$L(\xi) = \coth(\xi) - 1/\xi \tag{5}$$

$$\xi = \frac{\mu_0 mH}{k_B T} \tag{6}$$

where M is the ensemble magnetization in the direction of the applied field H and $L(\zeta)$ is the Langevin function. The value $n_m(m)$ in Eq. (4) represents the number density of MNP with a magnetic moment m per unit of MNP volume.

The measured *M-H* curve of the suspended SHP20 sample at low fields is represented with dots in Fig. 1(a). The value $M_s = 270$ kA/m was determined by the value of M at $\mu_0 H = 1$ T. The distribution of m in the MNP sample can be obtained from the experimental $M-H$ curve by solving the inversion problem given in Eq. (4) [9–11]. The inversion problem was solved numerically by using a mathematical technique called nonlinear-non-negative least square method (NNLS) [10].

The obtained $n_m(m)m^2$ vs. m curve for the SHP20 sample is shown in Fig. 1(b). As shown, the curve has main peak at $m = 1.4 \times 10^{-18}$ Am^2. Another sub peak is also obtained at $m = 2 \times 10^{-20}$ Am^2. Using Eq. (4), we can reconstruct the *M-H* curve from the obtained $nm(m)m^2$ vs. m curve. The reconstructed *M-H* is illustrated with the dotted line in Fig. 1(a) showing good agreement with the experimental *M-H* curve of suspended sample.

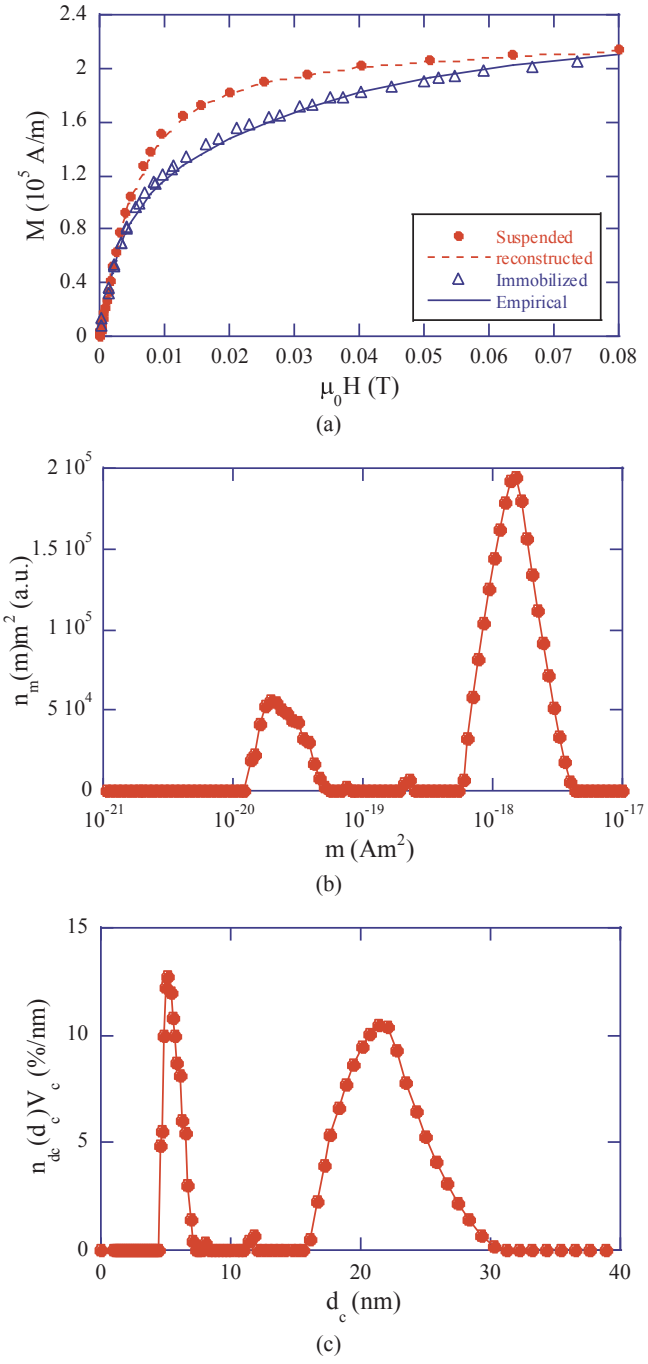

Fig. 1. (a) *M-H* curve of suspended and immobilized SHP20 samples and analytical results. (b) Magnetic moment distribution for SHP20 MNP. (c) Normalized core size distribution of SHP20 MNP.

The $n_m(m)m^2$ vs. m curve was then transferred to the distribution of d_c using the following relationship between $n_m(m)$ and number density of MNP with core size d_c per unit of MNP volume, $n_{d_c}(d_c)$:

$$n_{d_c}(d_c) = n_m(m) M_s \frac{\pi}{2} d_c^2 \tag{7}$$

Fig. 1(c) represents the estimated core size distribution obtained with $M_s = 270$ kA/m. The horizontal axis represents the diameter of the magnetic core d_c. The vertical axis represents the estimated volume-weighted core size distributions, $n_{d_c}(d_c)V_c$, normalized to 100%. As

shown, the $n_{d_c}(d_c)V_c$ vs. d_c curve has peaks at d_c = 5 and 21 nm, corresponding to the peaks in $n_m(m)m^2$ vs. m curve shown in Fig. 1(b). The value of d_c = 21 nm is consistent with the nominal size of 20 nm of the SHP20 sample. The curve also shows another peak at d_c = 5 nm. Such small core size may be explained by the incomplete crystallization of MNP [22]. We note that iron-oxide nanoparticles often suffer from a degraded magnetization which is caused by a magnetic dead layer and incomplete oxygenation of the core.

2.2. Magnetic anisotropy

In Fig. 1(a), the experimentally measured *M-H* curve of the immobilized SHP20 sample is represented with triangles. The value of K can be obtained by analyzing the immobilized sample *M-H* curve. For this purpose, we previously obtained an empirical expression for the *M-H* curve of immobilized MNP based on the numerical simulation results of the *M-H* curve using the energy expression including the anisotropy term [17]. The empirical expression for the magnetization, M_{Imm}, of the immobilized MNP is given by

$$M_{Imm} = gM_0 + (1 - g)M_\infty \tag{8}$$

where M_0 is the magnetization of suspended MNP given by Eq. (4). The value of M_∞ represent the magnetization of immobilized MNP in the case of infinite σ, and is given by

$$M_\infty = \int_0^\infty n_m(m) m_z(\xi, \sigma = \infty) dm \tag{9}$$

where

$$\frac{m_z(\xi, \sigma = \infty)}{m} = a_1 \tanh(b_1 \xi) + a_2 \tanh(b_2 \xi) + a_3 \tanh(b_3 \xi) \tag{10}$$

with the parameters a_1 = 0.3374, b_1 = 0.8225, a_2 = 0.1467, b_2 = 0.3703, a_3 = 0.0159, and b_3 = 0.0948.

The expression for g is

$$g = c_1 \tanh\left(d_1 \frac{H}{H_K}\right) + c_2 \tanh\left(d_2 \frac{H}{H_K}\right) + c_3 \tanh\left(d_3 \frac{H}{H_K}\right), \tag{11}$$

where,

$$\mu_0 H_k = \frac{2K}{M_s} \tag{12}$$

with the parameters c_1 = 0.893, d_1 = 1.27, c_2 = 0.04, d_2 = 0.228, c_3 = 0.067, and d_3 = 54.6.

The empirical expression given in Eq. (8) can be calculated using the distribution of $n_m(m)$ given in Fig. 1(b) and using H_K as an adjustable parameter. In Fig. 1(a), experimentally measured *M-H* curve of the immobilized SHP20 sample (triangles) is compared with the empirical expression (solid line). As shown, good agreement was obtained between calculated and experimental results when we choose $\mu_0 H_k$ = 50 mT. Note that the field range from $\mu_0 H$ = 20 to 80 mT corresponds to H/H_k = 0.4 to 1.6.

The value of K can be obtained using the relation given in Eq. (12). As M_s = 270 kA/m in the present sample, $\mu_0 H_k$ = 50 mT gives K = 6.8 kJ/m^3.

2.3. Characteristic relaxation time

The characteristic time τ_0, which determines the Néel relaxation time τ_N as given in Eq. (2), was obtained from the ACS of the immobilized MNP sample. In the experiment, weak external field with $\mu_0 H_{ac}$ = 0.1 mT was applied to satisfy the condition of magnetization linearity. The frequency of the excitation field was changed from 10 Hz to 100 kHz. The measurement was performed using equipment constructed in the laboratory.

In Fig. 2, the frequency dependence of ACS for the immobilized SHP20 sample is illustrated with triangles for the real part of the susceptibility, Re[*M(f)*]. The ACS measurement of suspended MNP sample is also plotted to show the difference between the suspended and immobilized case.

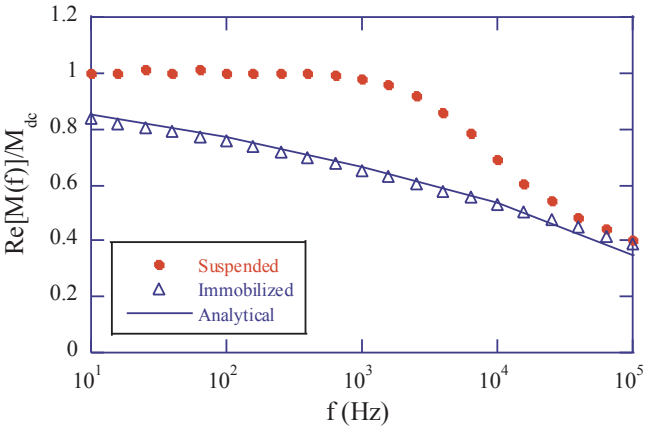

Fig. 2. Real part of the AC susceptibility of SHP20 samples. Symbols represent the experimental results. The solid line was calculated from Eq. (13) for $\tau_0 = 1 \times 10^{-10}$ s.

The value of τ_0 was estimated by analyzing the experimental results of immobilized sample by using the analytical relation previously explained in [23]

$$\frac{Re[M(f)]}{M_{dc}} = \frac{\int_0^\infty \frac{n_m(m)m^2}{1 + (2\pi f \tau_N)^2} dm}{\int_0^\infty n_m(m) m^2 dm} \tag{13}$$

The relation given in Eq. (13) can be calculated using the obtained distribution of $n_m(m)$ and K value while taking τ_0 value as an adjustable parameter. The solid line in Fig. 2 was calculated using Eq. (13) with $\tau_0 = 1 \times 10^{-10}$ s. As shown, good agreement between calculated and experimental results was obtained.

Using this estimation procedure, we obtained the SHP20 sample parameters M_s, $\mu_0 H_k$, K, and τ_0. These parameters are listed in Table 1. We also show the typical core diameter, denoted by d_{c_typ}, that gives the peak in the $n_{d_c}(d_c)V_c$ vs. d_c curve.

As shown in Figs. 1 and 2, magnetic properties reconstructed from the obtained parameters agree well with the experimental results. This agreement indicates the validity of the present procedure for parameters evaluation.

3. Resovist MNP parameter evaluation

Resovist MNP samples are known to have admirable performance in both hyperthermia and MPI applications. However, it has been shown that Resovist MNP samples have wide distribution of parameters [24]. Therefore, we fractionated Resovist MNP using magnetic fractionation [25,26]. The Resovist MNP were fractionated into two MNP samples, MS1 and MS3, with narrower core size distribution. The iron concentration of the original sample was 28 mg (Fe)/mL for these three MNP. Magnetic properties and parameters of fractionated MNP were compared to those of the original Resovist MNP.

The measured *M-H* curves of the suspended MS1, Resovist, and MS3

Table 1
Summary of magnetic parameters for the different MNP samples.

Sample	M_s (kA/m)	d_{c_typ} (nm)	$\mu_0 H_k$ (mT)	K (kJ/m^3)	τ_0 (s)
SHP20	270	21	50	6.8	1×10^{-10}
MS1	370	23	64.8	12.0	1×10^{-12}
MS3	250	7	40	5.0	1×10^{-12}
Resovist	300	7 & 26	53.3	8.0	1×10^{-12}

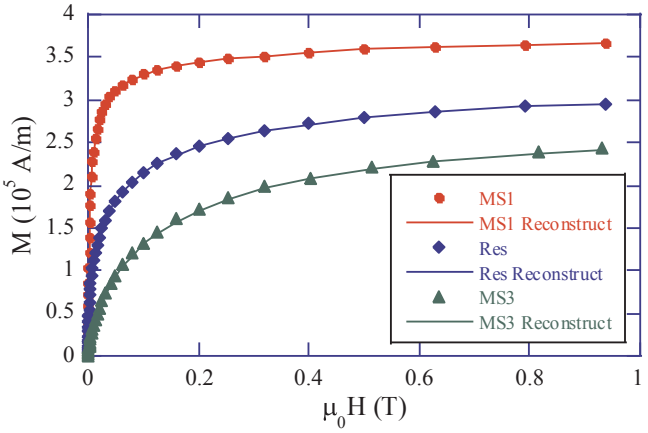

Fig. 3. *M-H* curve of suspended MS1, Resovist, and MS3 samples.

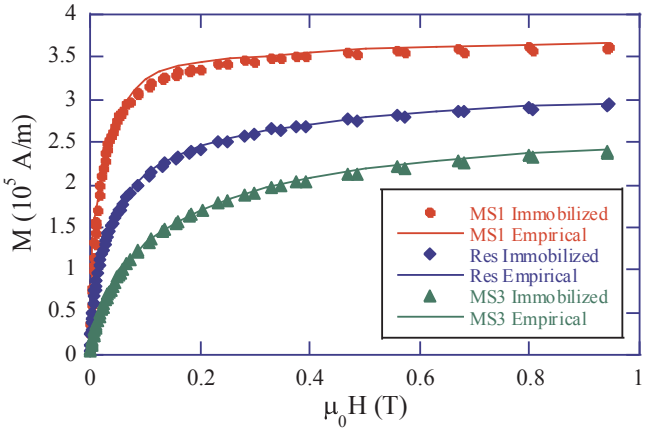

Fig. 5. *M-H* curve of immobilized MS1, Resovist, and MS3 samples.

samples are represented in Fig. 3 with circle, diamond, and triangle markers, respectively. MS1 had the highest value of M_s = 370 kA/m, the Resovist sample had M_s = 300 kA/m, and MS3 had M_s = 250 kA/m.

Using the procedure described in Section. 2.1, we obtained the core size distribution for each MNP sample. Fig. 4 illustrates the estimated size distributions for each MNP sample. As shown in Fig. 4, the Resovist sample had a wide size distribution with typical core sizes of d_{c_typ} = 7 nm and 26 nm. The MS1 sample had a narrower size distribution with typical core size around 23 nm, while MS3 sample had a smaller core size of 7 nm. The *M-H* curves reconstructed using the obtained magnetic moment distributions are illustrated with the solid lines in Fig. 3 showing good agreement with the experimental *M-H* curves.

The measured *M-H* curves of the immobilized MNP samples were compared to the empirical expression using the procedure given in Section 2.2. The solid lines in Fig. 5 represent the empirical expressions when the values of $\mu_0 H_k$ = 64.8, 53, and 40 mT were chosen for MS1, Resovist, and MS3, respectively. As shown, good agreement was obtained between the empirical and experimental results. Using the M_s and $\mu_0 H_k$ values, we obtained K = 12, 8, and 5 kJ/m^3 for MS1, Resovist, and MS3, respectively.

Fig. 6 shows the measured real parts of ACS as compared to the analytical expression evaluated from Eq. (13) for MS1, Resovist, and MS3 samples. The best fit between experimental and analytical results was obtained at $\tau_0 = 1 \times 10^{-12}$ s for the three samples.

We note that the difference in ACS between suspended and immobilized MS3 samples was caused by the large-diameter tail in the size distribution shown in Fig. 4. Particles with d_c 7 nm have very short relaxation time, and, therefore, no difference occurs between the suspended and immobilized cases for these particles.

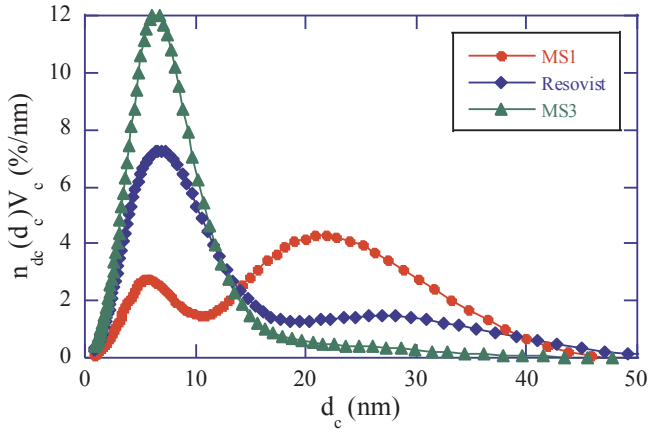

Fig. 4. Normalized core size distributions of MS1, Resovist, and MS3 samples. Distributions are estimated from *M-H* curves of suspended MNP samples.

Table 1 shows the summary of parameters evaluated for the Resovist, MS1, and MS3 MNP samples. As shown, the MS1 sample showed the largest values of M_s, H_k and K, while the MS3 sample showed the smallest values. On the other hand, characteristic time τ_0 was the same among the three samples.

We note that τ_0 can be expressed as [20]

$$\tau_0 = \frac{M_s}{2K}\frac{1}{\alpha\gamma} = \frac{1}{\mu_0 H_k}\frac{1}{\alpha\gamma} \tag{14}$$

where, $\gamma = 1.76 \times 10^{11}(\mathrm{sT})^{-1}$ is gyromagnetic ratio and α is the dimensionless damping factor. Substituting the estimated H_k value listed in Table 1, we obtain the τ_0 value of the SHP20 sample as $\tau_0 = 1.1 \times 10^{-9}$ s for typical value of α = 0.1. The τ_0 value obtained from the ACS experiment ($\tau_0 = 1 \times 10^{-10}$ s) was not significantly different from that calculated from Eq. (14).

On the other hand, for the case of multi-core MNP sample (Resovist, MS1 and MS3), the estimated τ_0 values ($\tau_0 = 1 \times 10^{-12}$ s) were much smaller than the value (τ_0 1×10^{-9} s) calculated with Eq. (14). This difference may be explained if we take the interactions between the cores into account for the multi-core MNPs samples, as shown in Ref. [21]: It was shown that the magnetic interaction between particles decreases the effective τ_0 value and increases the effective K value.

Next, we discuss the relationship between the obtained parameters of the original and fractionated samples. We note that the original Resovist sample is a mixture of MS1 and MS3 samples with certain portion of each sample. We first evaluate the portion of MS1 and MS3 MNPs in the Resovist sample using the M_s values of the three samples. As was shown previously, the M_s values were 300, 370, and 250 kA/m for the Resovist, MS1, and MS3 samples, respectively. When the portion of MS1 MNP is given by a, the portion of MS3 MNP is given by $1 - a$. Therefore, the M_s value of the Resovist sample is given by the volume-weighted average of the MS1 and MS3 samples as $300 = a \times 370 + (1 - a) \times 250$. Therefore, we obtain $a = 0.42$. This means that the original Resovist sample contains 42% MS1 and 58% MS3 MNP.

Using the estimated value of a, we can find the value of K of a mixture of MS1 and MS3 MNP. As the K values are 12 and 5 kJ/m^3 for MS1 and MS3, respectively, the volume-weighted average of K is given by $K = a \times 12 + (1 - a) \times 5 = 7.97$ kJ/m^3. This value agrees well with K obtained for the Resovist sample (K = 8 kJ/m^3). Similarly, H_k value of the mixture is given by $\mu_0 H_k = a \times 64.8 + (1 - a) \times 40 = 50.3$ mT. This value agrees with the $\mu_0 H_k$ value obtained for the Resovist sample ($\mu_0 H_k$ = 53.3 mT).

The above results indicate that the parameters of the Resovist sample are given by the volume-weighted average of the two

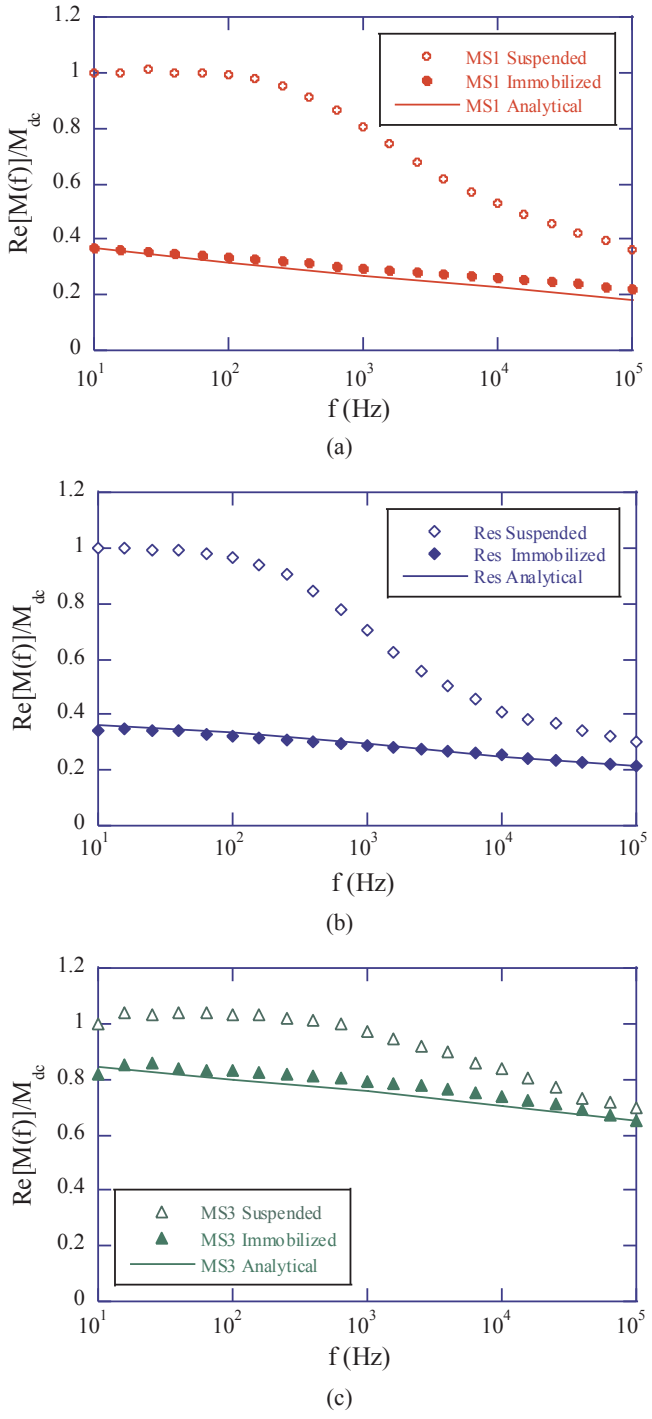

Fig. 6. AC susceptibility of immobilized (a) MS1, (b) Resovist, and (c) MS3 samples and the analytical result.

fractionated samples.

We note that the different values of M_s and K for the MS1 and MS3 samples indicate that these values are not constant in the MNP sample but change with the core size d_c of particles. Therefore, strictly speaking, we have to take the dependence of K and M_s on d_c into account. However, for simplicity, we assumed constant values of K and M_s in the sample for the evaluation procedure given in Section 2. Therefore, the parameters obtained with the present procedure represent the averaged values in each sample.

Finally, we estimated the m and τ_N values of MNP samples using parameters listed in Table 1. Fig. 7 shows the relationship between

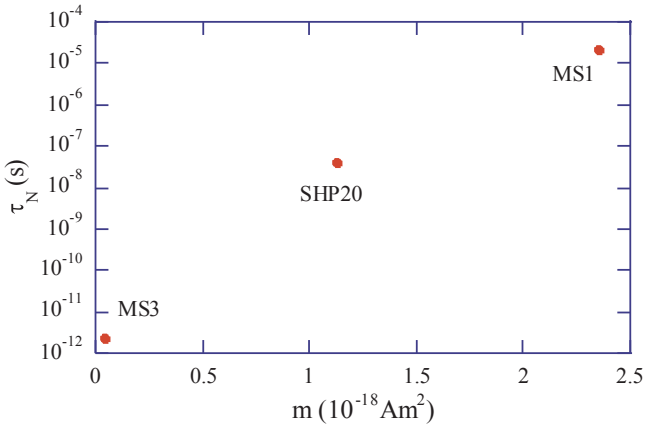

Fig. 7. Values of m and τ_N estimated for SHP20, MS1, and MS3 samples for typical core size d_{c_typ} listed in Table 1.

typical values of m and τ_N calculated using typical core size d_{c_typ} of SHP20, MS1, and MS3 samples. When we take the distribution of d_c into account, the m and τ_N values exist around these typical values. The results shown in Fig. 7 are useful for the selection of MNP with appropriate values of m and τ to be used in specific biomedical applications. We note, however, that it is necessary to collect more data, which will be our future work.

4. Conclusions

We demonstrated a procedure for estimating the magnetic parameters of MNP samples (M_s, d_c, K, and τ_0) from independent experimental measurements, namely, suspended sample M-H curve, immobilized sample M-H curve and ACS measurements. Using these parameters, we can obtain magnetic moment m and Néel relaxation time τ_N of a sample, which determine MNP performance in biomedical applications.

The proposed estimation procedure can be useful for the selection of MNP appropriate for specific applications. For example, among four studied MNP samples, the MS1 sample was the most suitable for the MPI application because it had large m and appropriate τ_N for the AC field with a frequency around 10 kHz.

Acknowledgments

This work was supported in part by a Grant-in-Aid for Scientific Research (S) JP15H05764, Japan Society for the Promotion of Science, Japan.

References

[1] R. Rosensweig, Heating magnetic fluid with alternating magnetic field, J. Magn. Magn. Mater. 252 (2002) 370–374, https://doi.org/10.1016/S0304-8853(02)00706-0.
[2] B. Gleich, J. Weizenecker, Tomographic imaging using the nonlinear response of magnetic particles, Nature. 435 (2005) 1214–1217, https://doi.org/10.1038/nature03808.
[3] Q.A. Pankhurst, N.T.K. Thanh, S.K. Jones, J. Dobson, Progress in applications of magnetic nanoparticles in biomedicine, J. Phys. D. Appl. Phys. 42 (2009), https://doi.org/10.1088/0022-3727/42/22/224001 224001.
[4] K.M. Krishnan, Advances in magnetics biomedical nanomagnetics: a spin through possibilities in imaging, diagnostics, and therapy, IEEE Trans. Magn. 46 (2010) 2523–2558, https://doi.org/10.1109/TMAG.2010.2046907.
[5] J. Carrey, B. Mehdaoui, M. Respaud, Simple models for dynamic hysteresis loop calculations of magnetic single-domain nanoparticles: application to magnetic hyperthermia optimization, J. Appl. Phys. 109 (2011) 83921, https://doi.org/10.1063/1.3551582.
[6] F. Ludwig, D. Eberbeck, N. Löwa, U. Steinhoff, T. Wawrzik, M. Schilling, L. Trahms, Characterization of magnetic nanoparticle systems with respect to their magnetic particle imaging performance, Biomed. Tech. Eng. 58 (2013) 535–545, https://doi.org/10.1515/bmt-2013-0013.

[7] T. Yoshida, N.B. Othman, K. Enpuku, Characterization of magnetically fractionated magnetic nanoparticles for magnetic particle imaging, J. Appl. Phys. 114 (2013), https://doi.org/10.1063/1.4829484.
[8] F. Ludwig, C. Balceris, T. Viereck, O. Posth, U. Steinhoff, H. Gavilan, R. Costo, L. Zeng, E. Olsson, C. Jonasson, C. Johansson, Size analysis of single-core magnetic nanoparticles, J. Magn. Magn. Mater. 427 (2017) 19–24, https://doi.org/10.1016/j.jmmm.2016.11.113.
[9] D.V. Berkov, P. Gönert, N. Buske, C. Gansau, J. Mueller, M. Giersig, W. Neumann, D. Su, New method for the determination of the particle magnetic moment distribution in a ferrofluid, J. Phys. D Appl. Phys. 33 (2000) 331–337.
[10] J. Van Rijssel, B.W.M. Kuipers, B.H. Erné, Non-regularized inversion method from light scattering applied to ferrofluid magnetization curves for magnetic size distribution analysis, J. Magn. fsMagn. Mater. 353 (2014) 110–115, https://doi.org/10.1016/j.jmmm.2013.10.025.
[11] P. Bender, C. Balceris, F. Ludwig, O. Posth, L. Bogart, W. Szczerba, A. Castro, L. Nilsson, R. Costo, H. Gavilán, D. González-Alonso, I. Pedro, L. Barquín, C. Johansson, Distribution functions of magnetic nanoparticles determined by a numerical inversion method, New J. Phys. 19 (2017) 73012.
[12] C. de Julián Fernández, Influence of the temperature dependence of anisotropy on the magnetic behavior of nanoparticles, Phys. Rev. B. 72 (2005) 54438, https://doi.org/10.1103/PhysRevB.72.054438.
[13] P.P. Vaishnava, R. Tackett, A. Dixit, C. Sudakar, R. Naik, G. Lawes, Magnetic relaxation and dissipative heating in ferrofluids, J. Appl. Phys. 102 (2007) 63914, https://doi.org/10.1063/1.2784080.
[14] G.T. Landi, F.R. Arantes, D.R. Cornejo, A.F. Bakuzis, I. Andreu, E. Natividad, AC susceptibility as a tool to probe the dipolar interaction in magnetic nanoparticles, J. Magn. Magn. Mater. 421 (2017) 138–151, https://doi.org/10.1016/j.jmmm.2016.08.011.
[15] M. Hanson, C. Johansson, S. Morup, The influence of magnetic anisotropy on the magnetization of small ferromagnetic particles, J. Phys. Condens. Matter. 5 (1993) 725 http://stacks.iop.org/0953-8984/5/i=6/a=009.
[16] V. Schaller, G. Wahnström, A. Sanz-Velasco, P. Enoksson, C. Johansson, Monte Carlo simulation of magnetic multi-core nanoparticles, J. Magn. Magn. Mater. 321 (2009) 1400–1403, https://doi.org/10.1016/J.JMMM.2009.02.047.
[17] A.L. Elrefai, T. Sasayama, T. Yoshida, K. Enpuku, Empirical expression for DC magnetization curve of immobilized magnetic nanoparticles for use in biomedical applications, AIP Adv. 8 (2018) 56803, https://doi.org/10.1063/1.5004725.
[18] I. Sato, M. Umemura, K. Mitsudo, M. Kioi, H. Nakashima, T. Iwai, X. Feng, K. Oda, A. Miyajima, A. Makino, M. Iwai, T. Fujita, U. Yokoyama, S. Okumura, M. Sato, H. Eguchi, I. Tohnai, Y. Ishikawa, Hyperthermia generated with ferucarbotran (Resovist®) in an alternating magnetic field enhances cisplatin-induced apoptosis of cultured human oral cancer cells, J. Physiol. Sci. 64 (2014) 177–183, https://doi.org/10.1007/s12576-014-0309-8.
[19] J. Haegele, R.L. Duschka, M. Graeser, C. Schaecke, N. Panagiotopoulos, K. Lüdtke-Buzug, T.M. Buzug, J. Barkhausen, F.M. Vogt, Magnetic particle imaging: kinetics of the intravascular signal in vivo, Int. J. Nanomed. 9 (2014) 4203–4209, https://doi.org/10.2147/IJN.S49976.
[20] W.T. Coffey, P.J. Cregg, Y.U.P. Kalmykov, On the theory of debye and néel relaxation of single domain ferromagnetic particles, Adv. Chem. Phys. Wiley-Blackwell, 2007, pp. 263–464, , https://doi.org/10.1002/9780470141410.ch5.
[21] J.L. Dormann, D. Fiorani, E. Tronc, Magnetic relaxation in fine-particle systems, Adv. Chem. Phys. Wiley-Blackwell, 2007, pp. 283–494, , https://doi.org/10.1002/9780470141571.ch4.
[22] J. Rijssel, B.W.M. Kuipers, B.H. Erné, Bimodal distribution of the magnetic dipole moment in nanoparticles with a monomodal distribution of the physical size, J. Magn. Magn. Mater. 380 (2015) 325–329, https://doi.org/10.1016/j.jmmm.2014.09.058.
[23] K. Enpuku, T. Sasayama, T. Yoshida, Estimation of magnetic moment and anisotropy energy of magnetic markers for biosensing application, J. Appl. Phys. 119 (2016), https://doi.org/10.1063/1.4948951.
[24] T. Yoshida, K. Enpuku, F. Ludwig, J. Dieckhoff, T. Wawrzik, A. Lak, M. Schilling, Characterization of resovist® nanoparticles for magnetic particle imaging, Springer Proc. Phys. Springer Berlin Heidelberg, 2012, pp. 3–7, , https://doi.org/10.1007/978-3-642-24133-8_1.
[25] N. Löwa, P. Knappe, F. Wiekhorst, D. Eberbeck, A.F. Thünemann, L. Trahms, Hydrodynamic and magnetic fractionation of superparamagnetic nanoparticles for magnetic particle imaging, J. Magn. Magn. Mater. 380 (2015) 266–270, https://doi.org/10.1016/j.jmmm.2014.08.057.
[26] T. Yoshida, T. Nakamura, O. Higashi, K. Enpuku, Magnetic fractionation and characterization of magnetic nanoparticles for magnetic particle imaging, Jpn. J. Appl. Phys. 57 (2018) 80302 http://stacks.iop.org/1347-4065/57/i=8/a=080302.